Perovskite nanoparticles Cs_4PbBr_6 and $CsPbBr_3$: synthesis, analysis and peculiar optical properties

A.G. Son*[a], V.A. Gushina [a], A.A. Egorova[a], A.A. Arkhipenko[a], A.A. Korotkova[a], A.A. Sadovnikov[a], Yu. Shandarov [b], N. A. Bert[c], D. A. Ivanov [b], N. Ch. Petrov [b], S. A. Kozyukhin[a]

[a.]Kurnakov Institute of General and Inorganic Chemistry, Russian Academy of Science, 31 Leninskii pr., 119071 Moscow, Russian Federation.

[b.]Photochemistry Centre, Russian Academy of Science, 59 Leninskii pr., 119333 Moscow, Russian Federation.

[c.]Ioffe Institute, Russian Academy of Science, 26 Politekhnicheskaya st., 194021 St Petersburg, Russian Federation.

Abstract

All-inorganic perovskite $CsPbBr_3$ and Cs_4PbBr_6 nanoparticles are being intensively studied due to their unique properties and wide range of applications; however, however, the nature of their optical properties is not yet fully understood due to the difficulty of synthesis of single-phase nanoparticles. In this article we describe the features of the synthesis of single-phase particles and the results of their chemical and phase analysis. Using data on nanoparticle concentrations, we experimentally determined the absorption coefficient for both phases. It has been shown that nanoparticles of $CsPbBr_3$ and Cs_4PbBr_6 perovskites exhibit features of such optical characteristics as photoluminescence, optical band gap, including the region of weak absorption (Urbach tail), and action spectrum also. The experimental results can be explained within the framework of existing ideas about the band gap structure for perovskite materials.

Introduction

The use of hybrid organic-inorganic materials with the ABX_3 perovskite structure (A is the organic or inorganic cation, B is the lead cation, X is the halogen) based on lead halides as functional materials in photovoltaic devices such as perovskite solar cells, LEDs, and photodetectors attracts on account of the special importance of their optical and electronic properties, such as a high consumption coefficient, a decrease in the binding energy of excitons, the possibility of detecting a band gap, a high mobility of charge carriers, as well as a high frequency of defects[1-4]. Current studies show that the efficiency of solar cells based on perovskites is comparable to the efficiency of devices based on inorganic semiconductors and is characterized by a rapid growth rate of this value in photovoltaic devices. Over the past decade, the energy conversion efficiency of devices based on perovskite materials has increased from 3.8% to 25.7%[5,6]. A promising composition in terms of the stability are completely inorganic perovskites, in which the organic methylammonium cation is replaced by an inorganic one, for example, Cs+. The presence of cesium cation at A-site provides high crystallinity and structural stability, which ensures thermal and humidity stability of perovskite devices[7].

In addition to bulk perovskites, attention is also engaged to nanoparticles (NPs) of similar compositions obtained as a result of colloidal synthesis. The advantages of $CsPbX_3$ colloidal nanoparticles are such parameters as a wide absorption spectrum and a bright photoluminescence band in the visible spectral range, a large diffusion path length of photoexcited charge carriers, and the possibility of tuning the emission band by changing the nanoparticle composition and size. In particular, anion exchange leads to the NPs formation with a mixed halide composition, while the emission can cover the entire visible spectrum[8-10], and partial replacement of a lead cation with a manganese cation can lead to the appearance of a second emission band[11]. Depending on the composition and amount of the precursors, as well as on the conditions for the synthesis of perovskite NPs, structures of various dimensions can be formed, for example, three-dimensional (3D) and zero-dimensional (0D) structures[12,13].

The main reason that currently does not allow us to turn to laboratory prototypes of perovskite devices with outstanding characteristics typical for industrial production is the lack of stability under real operating conditions (light, humidity, temperature)[14]. For optical devices based on low-dimensional NPs with a perovskite structure, there is another additional factor that affects the stability – this is the increased chemical activity of a highly developed surface. The ionic nature of lead halide perovskites characterizes these compounds as chemically unstable in polar solvents[15]. Therefore, the selection of surfactants to stabilize NPs with the perovskite structure is more complicated than the ligands used to stabilize classical semiconductor nanocrystals (NCs) II-VI, III-V, and IV-VI. However, the high ionic mobility characteristic of perovskite NCs positions this material as promising in photovoltaics. The CsX – PbX_2 (X = Cl, Br) phase diagram contains several stable compounds, in particular, incongruent Cs_4PbX6 ternary compounds and congruent $CsPbX_3$ compounds, the structures of which are shown in Fig. 1. Perovskites of the A4BX6 type, in particular Cs_4PbBr_6, have a crystal structure in which the $[PbBr_6]^{2-}$ octahedra are isolated from each other by Cs^+ trigonal prisms, forming one-dimensional $[CsPbX_6]_n^{3-}$ chains. Such chains are additionally isolated from each other by dodecahedrons Cs^+ [16,17]. Perovskite $CsPbX_3$, on the other hand, has a more symmetrical simple cubic structure, where the corners of the $[PbX_6]^{4-}$ octahedra are interconnected[16]. $CsPbBr_3$ nanocrystals exhibit bright green emission and high luminescence quantum yield ~ 92.8%[18], as well as enhanced spontaneous emission[19,20]. The optical properties of Cs_4PbBr_6 nanoparticles have not been sufficiently studied, which is due to the difficulty of synthesizing pure particles of composition 416, and therefore there is currently no consensus on the luminescent properties, and, accordingly, various models are proposed. It was shown that this type of perovskite does not exhibit luminescence in a number of studies on the preparation of Cs_4PbBr_6 nanocrystals[13,16,21,22]. On the other hand, the authors of some studies assume that luminescence is possible due to the presence of defects, free halide vacancies, in the crystal, but this theory has not been experimentally confirmed[23-25].

One of the key characteristics for the study of nanoparticles is the value of the quantitative concentration in a colloidal solution. This parameter is necessary for modeling laboratory prototypes of optoelectronic devices based on nanocrystals, assessing the toxicity of nanoparticles, and when using these structures as biolabels[26-28]. Determining the concentration of semiconductor nanoparticles is a complex experimental problem. Currently, the most popular methods for determining the concentration of nanoparticles are thermogravimetric analysis and UV-visible spectroscopy. However, these two methods are not accurate and require comparison with direct methods for the quantification[29,30]. Also, the concentration of NPs in a colloidal solution can be determined using inductively coupled plasma atomic emission spectroscopy. This method of the substance quantitative determination is the most accurate with an error of ~ 10^{-2} mg/g. The disadvantages of this method are the sample complete destruction, and the impossibility of determining the remnants of unreacted components in the sample. Determining the substance concentration in a solution by electron spectroscopy is based on the dependence of light absorption on the concentration of the solute. Therefore, in order to apply this method, knowledge of the substance absorption coefficient is necessary. Experimentally, the intrinsic absorption coefficient for 8 nm $CsPbBr_3$ perovskite nanocrystals (NCs) was first determined by a group of scientists led by Kovalenko, Hens and coworkers by combining inductively coupled plasma mass spectrometry (ICPMS) and absorption spectroscopy[31]. Later, Hens et al. presented another study on the determination of the intrinsic absorption coefficient for $CsPbBr_3$ NCs with sizes less than 7 nm, in which the authors use the same approach[32]. Based on the results of two studies, it was proved that the intrinsic absorption coefficient of $CsPbBr_3$ NCs does not depend on the particle size, and its value is estimated at ~ 2×10^5 mol^{-1} [31,32].

The purpose of this study was to obtain Cs_4PbBr_6 nanoparticles without $CsPbBr_3$ impurity, as well as to examine the optical properties of the resulting colloidal solutions of nanoparticles and quantify the concentration of these nanoparticles in solutions.

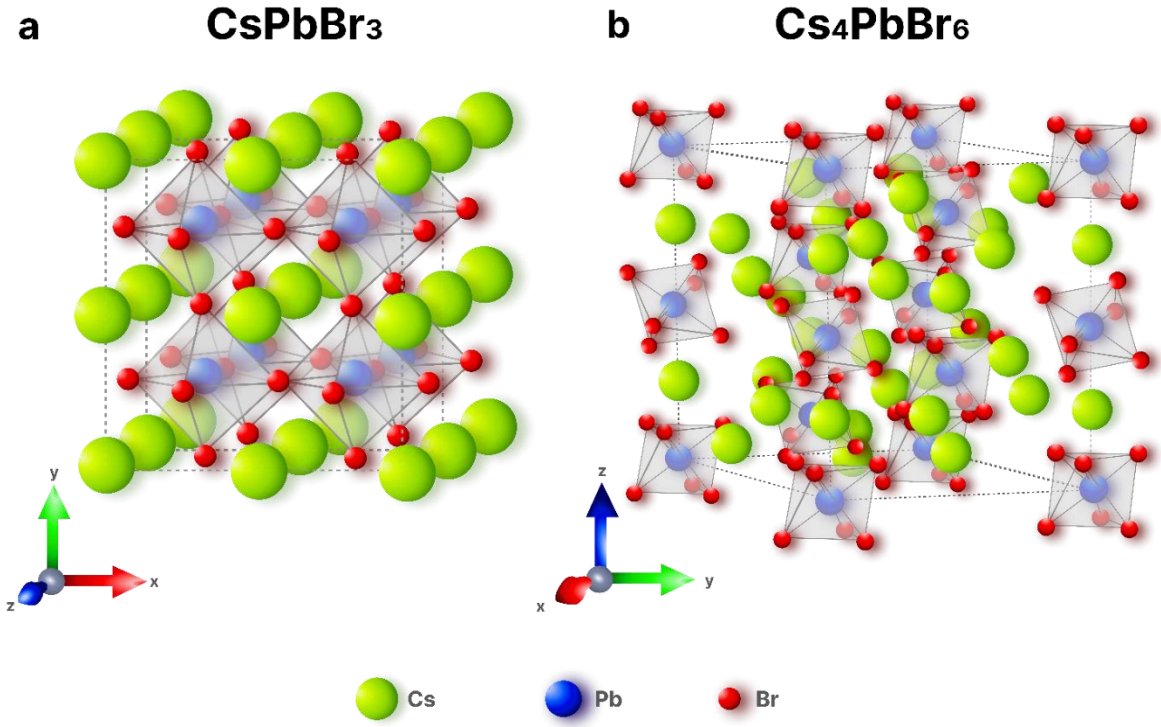

Fig. 1. Scheme of perovskite crystals (a) 3D phase and (b) 0D phase.

Experimental Section

Colloidal solutions of Cs_4PbBr_6 and $CsPbBr_3$ nanoparticles were obtained using modified hot injection[9] and sonication techniques[33].

Octadecene is the most popular high-boiling non-coordinating solvent in hot injection synthesis[9,31-33]. Mineral oil with a viscosity is eight times higher that of octadecene was chosen as the dispersion medium in given study. It is assumed that the replacement of the solvent with a more viscous one will make it possible to more effectively control the size of the resulting nanoparticles. According to the results of DLS analysis, the particles obtained in mineral oil have a smaller particle size than those obtained in octadecene under the same synthesis conditions (see SI, Fig. S2).

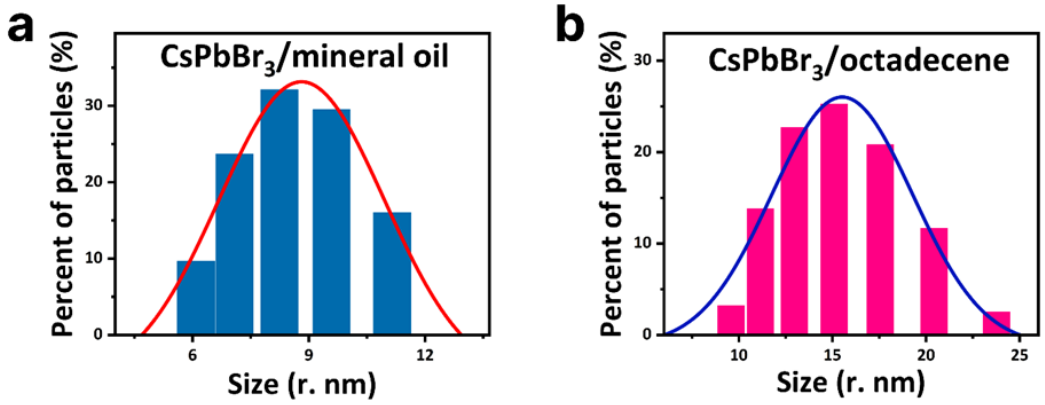

Fig. S2. DLS analysis of colloidal solutions $CsPbBr_3$ NPs obtained in (a) mineral oil and (b) octadecene.

Oleic acid (OA) and oleylamine (OAm), are commonly used as stabilizers[9,31-34]. Pan et al. investigated the effect of using various amines and carbon acids on the final product. This study shows, the combination of oleylamine with other long chain alkylamines as well as alkyl dithiols results in a stable colloidal solution with a narrow size dispersion[35]. Oleic acid and a mixture of oleylamine and pentadecylamine were used

as stabilizers in this study. We have previously shown that the use of pentadecylamine as a surfactant improved the optical properties of $CsPbI_3$ perovskite nanowafers[36].

Synthesis of $CsPbBr_3$ NPs

$CsPbBr_3$ nanoparticles (hereinafter 113) were obtained by injecting cesium oleate into a solution of lead bromide in a non-coordinating high-boiling solvent (mineral oil or octadecene) with a small amount of oleic acid, oleylamine, and pentadecylamine. After the introduction of cesium oleate, the colloidal solution was centrifuged, and then the precipitate was dispersed in a low-boiling solvent, n-hexane.

Synthesis of Cs_4PbBr_6 NPs

Cs_4PbBr_6 nanoparticles (416) were obtained by ultrasonic treatment (UT) at room temperature under ambient conditions. A mixture of cesium carbonate, lead bromide and stabilizers: oleic acid, oleylamine and pentadecylamine was dispersed in mineral oil using an ultrasonic homogenizer.

Results and discussions

$CsPbBr_3$ and Cs_4PbBr_6 NPs structure

The morphology of nanoparticles with the perovskite structure was studied using the analysis of transmission electron microscopy, presented in Figure 2 (b, e). The $CsPbBr_3$ sample (Fig. 2b), obtained by the hot injection method, is a cubic particle with a characteristic size of 6–13 nm, which is consistent with the results of the analysis performed by the STEM method (Fig. 2a, d). The Cs_4PbBr_6 sample (Fig. 1e) obtained by UT also represents particles of a cubic shape with sizes of 30–70 nm. In most particles, a pore about 5 nm in diameter is present in the center; there are particles with several pores. The main elements include Cs and Br, about 1 at. % Pb, which is confirmed by the EDX spectra (SI, Fig. S3 a, b). The absence of any peaks associated with impurity elements in the EDX spectra confirms the results of X-ray phase

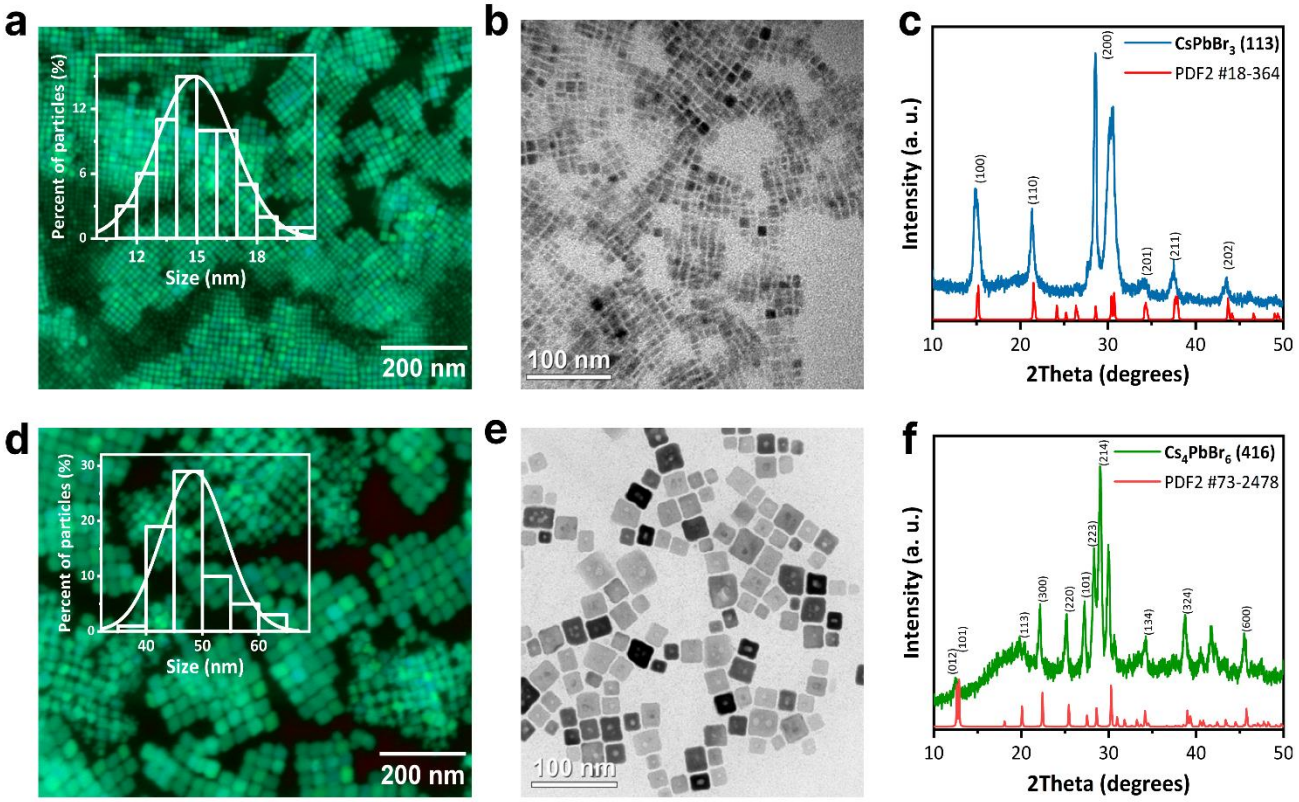

Fig. 2 (a, d) STEM images of (a) $CsPbBr_3$; (d) Cs_4PbBr_6. (b, e) TEM images of (b) $CsPbBr_3$; (e) Cs_4PbBr_6. (c, f) NPs XRD patterns of (c) $CsPbBr_3$ and (f) Cs_4PbBr_6.

analysis on the formation of a pure phase. The presence of oxygen and carbon is associated with the presence of stabilizers, and the copper signal refers to the material on which the particles were deposited. Figure 2 (c, f) shows the X-ray diffraction patterns of thin films of perovskite nanoparticles obtained. According to the XRD data, for the Cs_4PbBr_6 (416) composition, XRD reflexes are satisfactorily described by the rhombohedral structure of Cs_4PbBr_6, which belongs to the P2 group (PDF2 #73-2478). The structure of the $CsPbBr_3$ (113) sample has a monoclinic phase belonging to the R-3cr group (PDF2 #18-364). X-ray measurements show that both types of nanoparticles have good crystal quality without the presence of secondary phases, which is consistent with the results of the EDX analysis performed using TEM. The lattice parameters and unit cell volume for the rhombohedral and monoclinic phases extracted from the data shown in SI, Table S1.

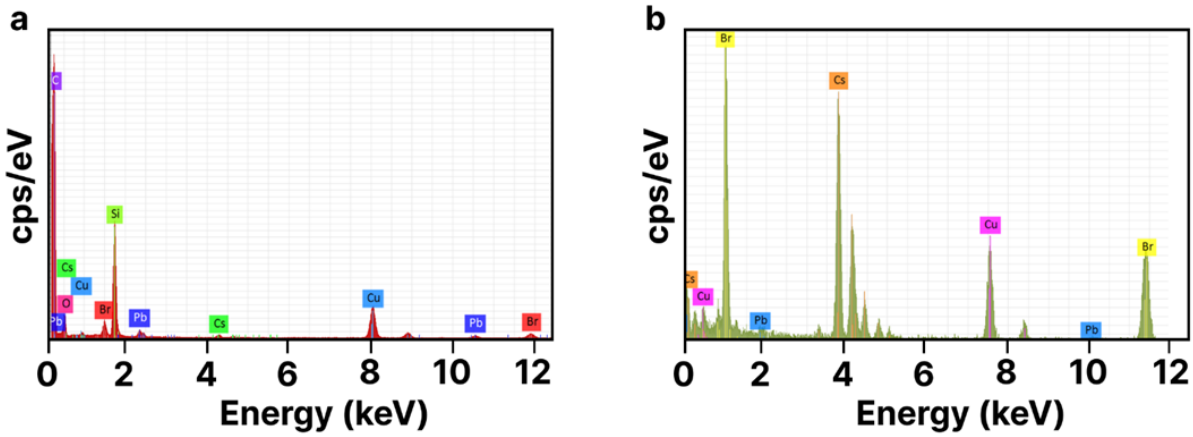

Fig. S3. EDX spectra of (a) $CsPbBr_3$ (113) and (b) Cs_4PbBr_6 (416).

Table S1. Lattice parameters for rhombohedral and monoclinic phases/Full profile analysis of diffraction patterns.

Rhombohedral		**Monoclinic**	
Cs_4PbBr_6 (416)		**$CsPbBr_3$ (113)**	
Parameter	**Value**	**Parameter**	**Value**
a	13,3683 Å	*a*	5,831 Å
		b	5,86 Å
		c	5,92 Å
Angle β	89,282°	Angle β	90°
Unit cell volume, Å^3			
2388,5		202,3	

Absorption spectra

The absorption spectrum of sample 416 (Fig. 3a) is characterized by the presence of two maxima at 225 nm and 313 nm. The absorption band at 313 nm corresponds to the absorption edge of Cs4PbBr6 NPs and can be attributed to the localized $^6S_{1/2} \rightarrow {}^6P_{1/2}$ transition inside individual $[PbBr_6]^{4-}$ octahedra separated by Cs+ ions[12,37]. Liu et al. asserts that the position of the absorption band does not change depending on the NP size, which confirms the assumption about $[PbBr_6]^{4-}$ octahedra isolated from each other in Cs_4PbBr_6 NPs[17]. A colloidal solution of NPs does not absorb in the visible range, which is consistent with the results obtained earlier for Cs_4PbBr_6 nanoparticles, as well as for crystals and thin films of this composition[12,34,38]. The $CsPbBr_3$ absorption spectrum (Fig. 3a) consists of several maxima, the position of which corresponds to the length waves 225, 260, 360 and 510 nm. The spectra of samples 416 and 113 show an absorption band at a wavelength of 225 nm. An identical maximum in the absorption spectrum was obtained for the Cs_4PbCl_6 crystal. S. Kondo et al. suggest that its presence can be attributed to the absorption of cesium ions[37].

$CsPbBr_3$ fluorescence spectra

A colloidal solution of $CsPbBr_3$ (113) has a bright fluorescence with an emission center at a wavelength of 518 nm (Fig. 3b). According to the data obtained, the position of the emission center does not depend on the concentration of NPs in the solution; however, with an increase in the aliquot in the solution, a linear increase in the sol fluorescence intensity is observed (SI, Fig. S4). No fluorescence was found in the Cs_4PbBr_6 (416) colloidal solution, which indicates the absence of emission centers and is consistent with experimental studies[12,38].

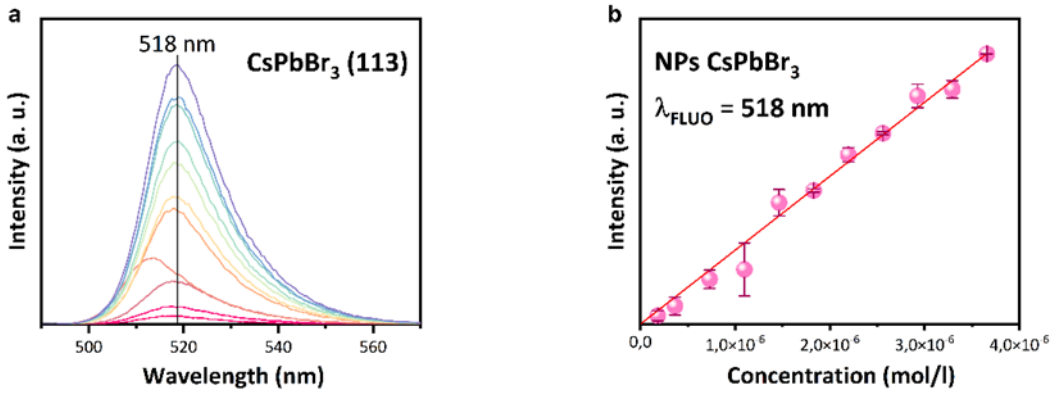

Fig. S4. (a) $CsPbBr_3$ fluorescence spectra for different NP concentrations in the range from 10^{-7} to 10^{-6} mol/l. (b) The dependence of the emission center intensity on the NP concentration.

$CsPbBr_3$ (113) action spectrum

To evaluate the efficiency of nonradiative transitions from the excited state of a fluorophore, one can use the absorption-fluorescence method[39]. The essence of this method is to compare the absorption and excitation spectra of fluorescence. The absorption spectrum measured by a spectrophotometer can be written as

$$A(\lambda) = \varepsilon(\lambda)cl \quad (1)$$

where $\varepsilon(\lambda)$ is the molar extinction coefficient, A is the absorption of colloidal solution, c is the fluorophore concentration, and l is the optical path length. Since relaxation from an excited state can occur both radiatively and nonradiatively, we can rewrite this expression as

$$A(\lambda) = [\varepsilon_f(\lambda) + \varepsilon_{nr}(\lambda)]cl \quad (2)$$

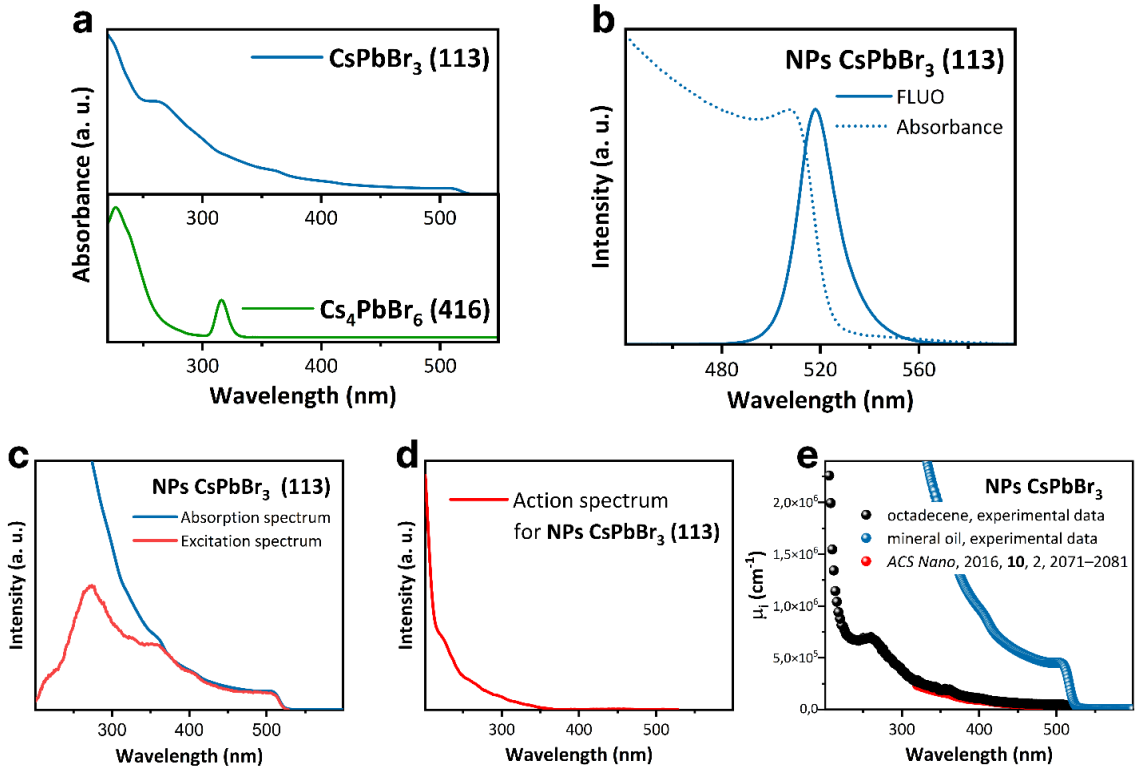

Fig. 3 (a) Absorption spectra of a colloidal solution. (b) CsPbBr3 fluorescence spectrum. (c) The absorption and excitation spectra of CsPbBr3 colloidal solution, (d) CsPbBr3 action spectrum. (e) The intrinsic absorption coefficient of $CsPbBr_3$.

where $\varepsilon_f(\lambda)$ and $\varepsilon_{nr}(\lambda)$ have the meaning of the radiative and nonradiative relaxation cross sections, respectively. In this case, the fluorescence excitation spectrum is proportional to the first term:

$$F(\lambda) \sim \varepsilon_f(\lambda) cl \tag{3}$$

which allows us to represent the absorption spectrum as the sum of two terms:

$$A(\lambda) = kF(\lambda) + Act(\lambda) \tag{4}$$

here k is a wavelength-independent coefficient describing possible losses in the spectrophotometer, $F(\lambda)$ is the fluorescence excitation spectrum, and $Act(\lambda) = \varepsilon_{nr}(\lambda)$ is the action spectrum responsible for fast nonradiative transitions from the excited state. The coefficient k must be such that the excitation spectrum nowhere exceeds the absorption spectrum, which follows from the law of conservation of energy.

On Fig. 3c shows the absorption spectrum and normalized excitation spectrum of $CsPbBr_3$ (113). Their difference is an action spectrum (see Fig. 3d), which exhibits several minor peaks in the 350-500 nm region, and increases very rapidly in the ultraviolet part of the spectrum, which may be due to non-radiative transitions in the cesium atom. The action spectrum minimum, which determines the excitation wavelength with the maximum fluorescence quantum yield, corresponds to 375 nm.

For a qualitative assessment of the losses associated with nonradiative transitions, one can introduce the quantity:

$$q_{nr} = \frac{\int Act(\lambda)d\lambda}{\int Abs(\lambda)d\lambda} \quad (5)$$

In the range from 375 to 530 nm, this value is about 0.1; however, for the entire absorption spectrum (200 – 530 nm), q_{nr} increases to ~ 0.7 due to the significant contribution of nonradiative processes in the region of 200 – 350 nm.

Determination of the molar concentration and the intrinsic absorption coefficient of colloidal solutions

One of the problems of colloidal nanoparticle solutions is to determine the concentration of the components that make up the solution. The well-known method of determining the concentration of chemical elements is mass spectroscopy, which allows to determine this parameter with low error values. However, concentration determination by mass spectrometry is a labour-intensive and technically difficult task. In our study it was proposed to combine inductively coupled plasma atomic emission spectroscopy (ICP-AES) and X-ray fluorescence elemental analysis (XRF) with UV-visible spectroscopy in such a way as to minimize the use of mass spectroscopy.

One of the well-known methods for concentration determination of nanoparticles is the UV-visible spectroscopy. According to the Lambert-Beer law, the absorption of light in colored solutions depends on the concentration of the solute[40].

$$A = \varepsilon cL \quad (6)$$

where A is the absorption, c is the molar concentration, L is the optical path length и ε is the molar absorption coefficient. A similar dependence is also observed for colloidal solutions of semiconductor nanoparticles. Thus, the concentration of a colloidal solution can be found if the molar absorption coefficient ε is known. The expression for the absorption coefficient of colloidal solutions of semiconductor nanoparticles is based on the Maxwell-Garnett effective medium theory within the local field approximation41 and can be determined by equation 7.

$$\varepsilon = \frac{N_A V_{QD}}{ln10}\mu_i \quad (7)$$

where μ_i is the intrinsic absorption coefficient, N_A is Avogadro number, V_{QD} is quantum dot volume. By definition μ_i is related to the absorption of the colloidal solution A, the concentration of nanoparticles f and the optical path length L [31,32,41].

$$\mu_i = \frac{\ln 10A}{fL} \quad (8)$$

The NPs concentration f depends on the molar concentration of the colloidal solution and the lattice constant of perovskite nanoparticles and can be calculated by the equation:

$$f = \frac{c \times N_A \times a}{10^{24}} \quad (9)$$

where c is the molar concentration of colloidal solution, N_A is Avogadro number, a is the unit cell volume.

M. Kovalenko and Hens determine the intrinsic absorption coefficient for semiconductor nanoparticles of $CsPbBr_3$ composition depending on the particle size from 6 to 11 nm. According to these results, it was

found that μ_i does not depend on the size of semiconductor NPs in separate wavelength regions, 325-345 nm and 415-455 nm[31,32,41]. This approach is also applicable to more complex nanocrystals, such as core/shell heteronanocrystals, nanorods, nanowires, or nanoplates[28,42-44]. Knowing the intrinsic absorption coefficient makes it possible to understand the mechanism of NP synthesis kinetics, the photoluminescence processes of single nanocrystals, and also to evaluate the possibility of enhancing the optical characteristics of devices based on semiconductor NPs[24,45,46].

The ratio of the main components of the sols was established using the method of fundamental parameters (Table 1). Based on the obtained XRF data (see SI, Fig. S5), it was found that the ratio of elements by fundamental parameter method (FPM). The ratio of CsxPbyBrz for colloidal solution 113 is equal to $CsPb_{1.2}Br_{2.5}$, and for solution 416 – $Cs_{8.5}PbBr_{7.5}$. The high content of cesium and bromine in colloidal solution 416 may be due to the presence of side products, cesium oleate and cesium bromide.

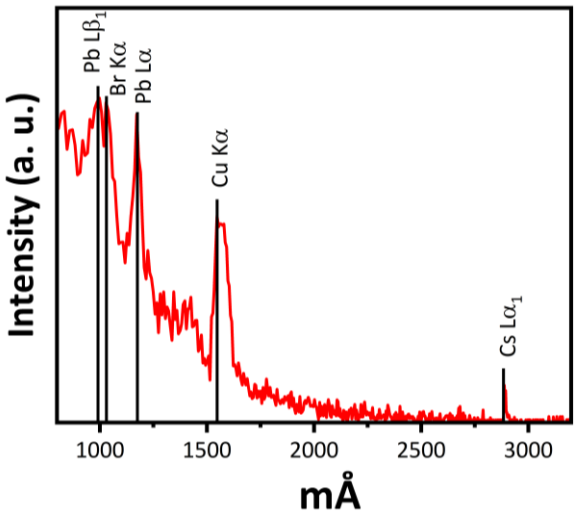

Fig. S5. X-ray fluorescence spectrum of $Cs_xPb_yBr_z$ colloidal solutions.

To determine the exact value of lead concentration content in the obtained samples, the resulting colloidal solution of nanoparticles was transferred to a true solution by dissolving the nanoparticles in a mixture of hydrochloric and nitric acids, followed by separation of the organic phase in a separating funnel. The separated solution was made up to the mark with deionized water. For analysis by the ICP-AES method, the samples were additionally diluted by a factor of 10. The analytical lines of the element being determined were chosen by conducting a preliminary experiment on model solutions. The selection criterion was the possibility of taking into account the background in the vicinity of the line. To determine

Table 1 The results of X-ray fluorescence analysis obtained using the FPM method.

Sample	Element	Mass fraction, %
$CsPbBr_3$ (113)	Cs	23,85 ± 1,54
	Pb	41,78 ± 3,32
	Br	34,37 ± 3,42
$CsPbBr_3$ (octadecene)	Cs	30,40 ± 3,41
	Pb	36,75 ± 1,86
	Br	32,48 ± 1,11
Cs_4PbBr_6 (416)	Cs	58,08 ± 5,1
	Pb	10,85 ± 2,53
	Br	31,07 ± 4,43

Table 2 Results of determination of lead concentration by AES-MS methods.

Sample	Element	Concentration, mg/l
Cs_4PbBr_6 (416)	Pb	174,92 ± 0,07
$CsPbBr_3$ (113)	Pb	22,17 ± 0,05
$CsPbBr_3$ (octadecene)	Pb	20,08± 0,05

the Pb concentration, the following analytical lines were chosen: 220.353 nm, 216.999 nm and 261.418 nm. The limits of determination were calculated using the 3S test and amounted to 0.002–0.010 depending on the analytical line. The results of the analysis of $Cs_xPb_yBr_z$ samples by AES-MS are shown in Table 2.

To calculate the intrinsic absorption coefficient, series of electron absorption spectra of colloidal solutions were recorded depending on the NPs concentration. The dependences of absorption values on the NPs concentration were plotted based on experimental results (SI, Fig. S6 a, b). One can see that these dependencies are linear, which makes it possible to apply the Lambert-Beer law to calculate μi of colloidal solutions (SI, Fig. S6 c, d). The calculated values of the intrinsic absorption coefficient (Eq. 8) are shown in Table 3.

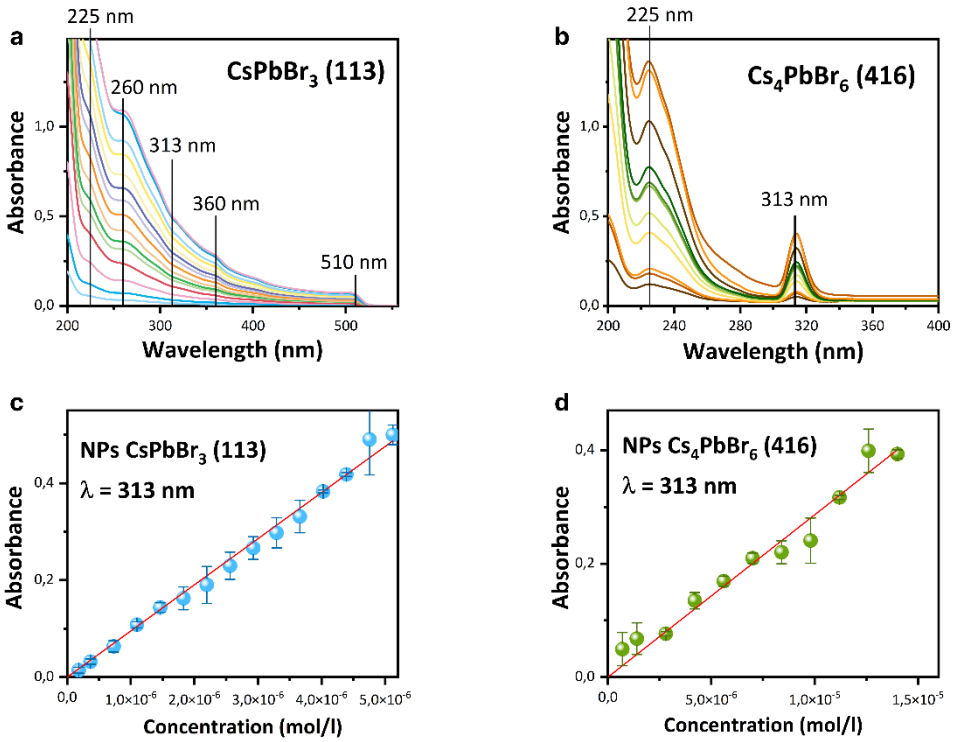

Fig. S6. (a, b) Absorption spectra of a colloidal solutions. (c, d) Dependence of absorption on NPs concentration at λ = 313 nm.

The absorption coefficient calculated for λ = 335 nm, so this section of the spectrum does not depend on the size of the nanostructures[31,32,41]. Table 4 shows the μ_i values of the sols calculated for λ = 335 nm, as well as for λ = 313 nm and 360 nm, corresponding to the characteristic absorption maxima of the samples.

Estimating the absorption coefficient for a colloidal solution is a rather difficult task. To establish the true value of the absorption coefficient of $CsPbBr_3$ NPs, colloidal solutions were synthesized using the classical non-coordinating solvent octadecene ($CsPbBr_3$ octadecene) and mineral oil ($CsPbBr_3$ 113). It was found that the use of mineral oil leads to a tenfold increase in the absorption coefficient, which is an indicator

Table 3 Evaluation of the intrinsic absorption coefficient

Sample	$\mu_{i\,(225\ nm)}$, cm^{-1}	$\mu_{i\,(313\ nm)}$, cm^{-1}	$\mu_{i\,(335\ nm)}$, cm^{-1}	$\mu_{i\,(400\ nm)}$, cm^{-1}
Cs_4PbBr_6 (416)	$(1{,}51\pm0{,}05)\times10^5$	$(1{,}7\pm0{,}11)\times10^3$		
$CsPbBr_3$ (113)	$(6{,}23\pm0{,}06)\times10^6$	$(1{,}74\pm0{,}07)\times10^6$	$(1{,}3\pm0{,}05)\times10^6$	$(5{,}42\pm0{,}07)\times10^5$
$CsPbBr_3$ (octadecene)	$(7{,}63\pm0{,}1)\times10^5$	$(3{,}04\pm0{,}09)\times10^5$	$(2{,}29\pm0{,}05)\times10^5$	$(1{,}09\pm0{,}07)\times10^5$
$CsPbBr_3$ Error! Bookmark not defined.			2×10^5	$0{,}9\times10^5$
$CsPbBr_3$ Error! Bookmark not defined.			$1{,}6\times10^5$	$0{,}8\times10^5$

of the interaction of the NP surface with mineral oil. We assume that mineral oil in this case plays the role of not only a solvent, but also the role of a surfactant, additionally stabilizing NPs in a colloidal solution. Therefore, the use of mineral oil in the synthesis process enhances the absorption of the colloidal solution of perovskite particles. The use of the method for estimating the absorption coefficient of semiconductor NPs[41], proposed by Hence, does not take into account the interaction of the solvent and NPs in a colloidal solution, and, therefore, is inaccurate.

The optical band gap of $CsPbBr_3$ and Cs_4PbBr_6 NPs

The fundamental quantity characterizing the applicability of a material as a photovoltaic device is the optical band gap E_g. To estimate this value from the experimental optical absorption spectra, the Tauc method was used, which describes the dependence of the absorption coefficient of a direct-gap semiconductor on the photon energy in the form of an equation47:

$$\alpha h\nu^x = B\left(h\nu - E_g\right) \tag{10}$$

where α is the absorption coefficient of the sample obtained from the electron absorption spectra, h is Planck's constant, ν is the photon frequency, x is the coefficient depending on the nature of the electronic transition, B is the coefficient depending on the substance concentration, E_g is the band gap of the semiconductor. In our study, we use the values of the intrinsic absorption coefficient μ_i calculated by the method proposed by Hens[41] taking them as α. Coefficient B was taken equal to 1, the effect of the solvent was not taken into account. The value of the exponent x for both $CsPbBr_3$ and Cs_4PbBr_6 is 1/2, which corresponds to the allowed direct optical transition. Thus, Tauc equation (10) takes the form:

$$\mu_i h\nu^x = B(h\nu - Eg) \tag{11}$$

where μ_i is the intrinsic absorption coefficient of the NPs.

Based on the results of UV-Vis spectrophotometry for NP samples 113 and 416, the dependence $[m_i h\vartheta]^{1/2} = f(h\vartheta)$ was plotted (Fig. 4 a, d). For each graph, a linear section was distinguished, which was extrapolated to the intersection with the x-axis; the intersection points of which corresponds to the value of the optical band gap. The values for the samples 113 were 2.34 eV, and 3.73 eV for 416. Previously, papers were published on the estimation of the band gap of crystals and thin films with the perovskite

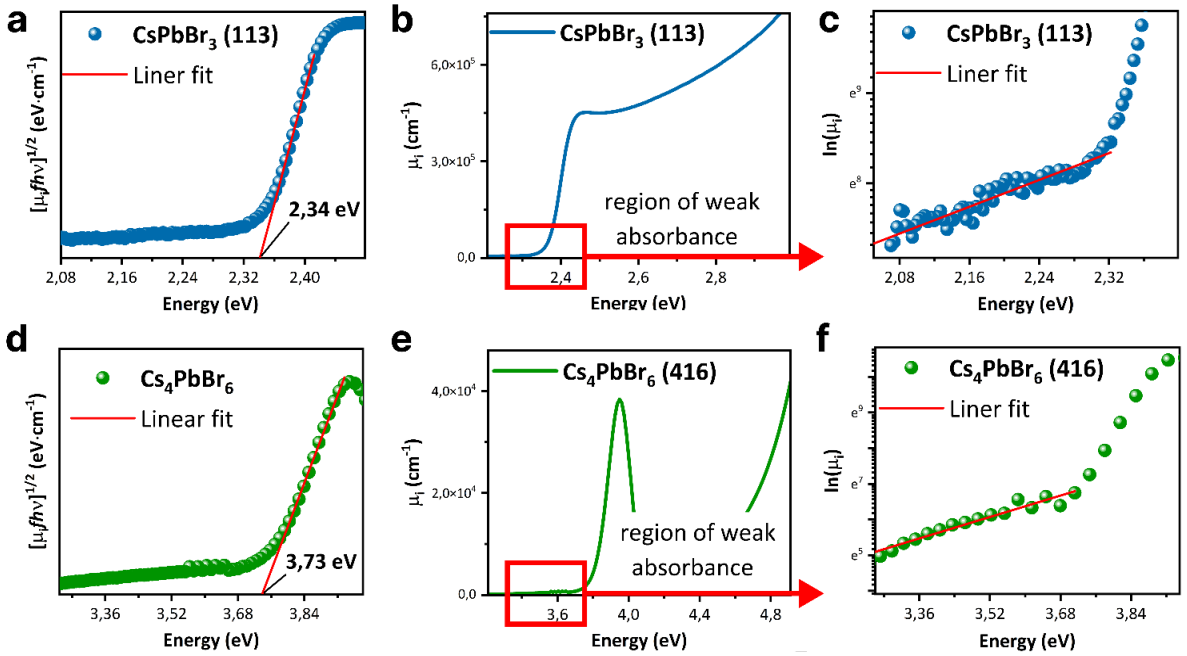

Fig. 4 (a, d) The optical band gap estimation of nanoparticles by Tauc method. (b, e) The intrinsic absorption coefficient dependence of energy. (c, f) The dependence of $ln(\mu_i)$ on energy.

structure $CsPbX_3$ and Cs_4PbX_6 by DFT methods. Thus, for $CsPbBr_3$ perovskites, the band gap is estimated as 3.26 eV, and 3.95 eV for Cs_4PbBr_6[48-50].

As can be seen from the dependence $\mu_i = f(h\vartheta)$ shown in Figure 4 (b, e), for both samples, an exponential dependence follows below the region of weak absorption. The area of exponential change in the extinction coefficient with increasing $h\vartheta$ is called Urbah tail, and it appears in the low crystalline, poor crystalline, the disordered and amorphous materials because these materials have localized tail states which extend in the band gap[51].

The sub-gap states contribute to the well-known tail states in non-crystalline solids, where the absorption coefficient is found empirically to depend exponentially on the energy below the conduction band edge. The steepness parameter is a major of the density of disorders present in the tail states and hence the Urbach energy depends on the energetic disorder and is one of the parameters that influences the rate of trap assisted recombination and perovskite solar cells (PSCs) performance.

Urbach law can be written as[52]:

$$\alpha(E) = \alpha_0 \exp\left[\frac{(E - E_0)}{E_U}\right] \tag{12}$$

where E_U is the Urbach energy, a characteristic quantity that characterizes the edge steepness E_0 is the energy associated with the band gap. The value E_0 can be defined as the minimum possible for a sample without defects[53-55]. These values are 2.34 eV for $CsPbBr_3$ NPs and 3.73 for Cs_4PbBr_6 NPs in our study.

We used the calculated values of the intrinsic absorption coefficient μ_i as α, the equation for the low-energy edge dependence of the absorption spectrum can be written as:

$$\mu_i(E) = \mu_0 \exp\left[\frac{(E - E_0)}{E_U}\right] \tag{13}$$

According to eq. 13, the value of E_U can be calculated by linear approximation of the dependence of $\log(\mu_i)$ in $h\vartheta$. The value of E_U for sample 113 is 7.3 meV, for sample 416 it is 190.1 meV. One can see that 416 NPs have a significantly higher Urbach energy compared to 113 NPs; we also identified that colloidal solutions of 416 NPs do not demonstrate noticeable FL at room temperature, in contrast to colloidal solutions of the composition $CsPbBr_3$ (113) which show bright green emission (see Fig. 3b).

It is well established that perovskites are known to suffer from a significant density of sub-gap states leading to non-negligible recombination losses[56-57]. It is also well known that in perovskite structures when free electrons and holes meet, they may form an exciton, which will dissociate again into free electrons and holes with high probability. Occasionally, the excitons (or free electrons and holes) recombine radiatively, leading to photoluminescence, or nonradiatively. It can be assumed that in the case of 416 NPs the electrons and holes spend significantly more time as free charge than bound as excitons, and the free electrons are hence susceptible to becoming trapped in defect sites, the density of states of which is large, resulting in nonradiative decay. If the density of defect states is reduced as in the case of 113 NPs with a low Urbach energy, the fractional time the charges spend bound as excitons increases, and the radiative recombination is realized during their dissociation. Hence, the competition for radiative decay increases with respect to charge trapping, leading to bright green emission.

Conclusions

Colloidal solutions of perovskite nanoparticles with compositions Cs_4PbBr_6 and $CsPbBr_3$ were obtained using modified methods of hot injection and UT. In this study provided alternative reaction conditions, in particular, classic high-boiling solvent octadecene was replaced by mineral oil; that was improved absorbance colloidal solutions. It was experimentally determined the intrinsic absorption coefficients of $CsPbBr_3$ obtained by in silicon oil and $CsPbBr_3$ and Cs_4PbBr_6 obtained by in octadecene, for $CsPbBr_3$ (113) the value was $(1.73\pm0.07) \times 10^6$ cm^{-1}, for $CsPbBr_3$ (octadecene) – $(2.29 \pm 0.05) \times 10^5$ cm^{-1}, Cs_4PbBr_6 (416) – $(1.70 \pm 0.11) \times 10^3$ cm^{-1}. Based on our results, the use of silicon oil promotes significant contribution to obtaining particles with high value of absorbance. Colloidal solutions of $CsPbBr_3$ exhibit bright luminescence with an emission centre at 518 nm, while Cs_4PbBr_6 does not exhibit emission in the ultraviolet and visible spectral ranges. Also, in this study, it was calculated optical band gap and Urbah tail energy. Cs_4PbBr_6 value of Urbah tail energy exceeds $CsPbBr_3$ value, that indicate the presence of a larger number of defect states in the band gap. If the density of defect states is lower, as in the case of 113 NPs with low Urbach energy, then the lifetime of excitons will be longer, and their dissociation will lead to emission. This provides important insights to the optical properties of perovskite based on lead, bromine and cesium.

Conflicts of interest

There are no conflicts to declare.

Acknowledgements

This study was supported by grunt of the Russian Science Foundation (№ 21-19-00853) and was performed using the equipment of the JRC PMR IGIC RAS.

References

[1]J. Zhang, G. Hodes, Z. Jin, S. Liu and S. Liu, Angew. Chem. Int. Ed. 2019, 58, 15596.

[2]F. Chen, L. Xu, Y. Li, T. Fang, T. Wang, M. Salerno, M. Prato and J. Song, J. Mater. Chem. C, 2020, 8, 13445-13452.

[3]Y. He, M. Petryk, Z. Liu, D. Chica, I. Hadar, Ch. Leak, W. Ke, I. Spanopoulos, W. Lin, D. Chung, B. Wessels, Z. He and M. Kanatzidis, Nat. Photonics, 2021, 15, 36–42.

[4]Y. Zhang, A. Kirs, F. Ambroz, C.-T. Lin, A. Bati, I. Parkin, J. Shapter, M. Batmunkh and T. Macdonald, Small Methods, 2021, 5, 2000744.

[5]M. Green, E. Dunlop, J. Hohl-Ebinger, M. Yoshita, N. Kopidakis, K. Bothe, D. Hinken, M. Rauer and X. Hao, Prog. Photovolt: Res Appl., 2022, 30(7), 687–701.

[6]National renewable energy laboratory. Best research-cell efficiencies., (https://www.nrel.gov/pv/assets/pdfs/best-research-cell-efficiencies-rev220630.pdf)

[7]X. Meng, X. Tian, S. Zhang, J. Zhou, Y. Zhang, Z. Liu and W. Chen, Sol. RRL, 2022, 6, 2200280.

[8]H. J. Snaith, Nature Mater, 2018, 17, 372–376.

[9]L. Protesescu, S. Yakunin, M. Bodnarchuk, F. Krieg, R. Caputo, Ch. Hendon, R. Yang, A. Walsh and M. V. Kovalenko, Nano Lett. ASC, 2015, 15 (6), 3692-3696.

[10]Y. Sheng, A. Zhao, S. Yuan, C. Liu, X. Zhang, Y. Di and Z. Gan, New J. Chem. The RSC, 2020, 44, 20592-20599.

[11]L. Wu, Y. Wang, M. Kurashvili, A. Dey, M. Cao, M. Döblinger, Q. Zhang, J. Feldmann, H. Huang and T. Debnath, Angew. Chem. Int. Ed., 2022, 61(15), 202115852.

[12]S. Sun, M. Lu, J. Guo, F. Zhang, P. Lu, Y. Fu, X. Bai, Zh. Shi, Zh. Wu, W. Yu and Y. Zhang, Chemical Engineering Journal, 2022, 433 (2), 133556.

[13]Ch. Zhou, Y. Lee, J. Cha, B. Yoo, S.-P. Cho, T. Hyeon, and I. Chung, J. Am. Chem. Soc. ACS, 2018, 140, 29, 9282-9290.

[14]B. Finkenauer, Akriti, K. Ma and L. Dou, ACS Appl. Mater. Interfaces, 2022, 14, 21, 24073–24088.

[15]Y. Kim, E. Yassitepe, O. Voznyy, R. Comin, G. Walters, X. Gong, P. Kanjanaboos, A. Nogueira and E. Sargent, ACS Appl. Mater. Interfaces, 2015, 7, 45, 25007–25013.

[16] Jun Yin, P. Maity, M. Bastiani, I. Dursun, O. Bakr, J.-L. Breds and O. Mohammed, Sci. Adv., 2017, 3, e1701793.

[17]Z. Liu, Y. Bekenstein, X. Ye, S. Nguyen, J. Swabeck, D. Zhang, S.-T. Lee, P. Yang, W. Ma and A. P. Alivisatos, J. Am. Chem. Soc., 2017, 139, 15, 5309–5312.

[18]Y. Li, M. Cai, M. Shen, Y. Cai and R.J. Xie, J. Mater. Chem. C., 2022, 10, 8356–8363.

[19]D. Yan, T. Shi, Z. Zang, T. Zhou, Z. Liu, Z. Zhang, J. Du, Y. Leng and X. Tang, Small, 15, 1901173–1901184.

[20]S. Yakunin, L. Protesescu, F. Krieg, M.I. Bodnarchuk, G. Nedelcu, M. Humer, G. De Luca, M. Fiebig, W. Heiss and M. V. Kovalenko, Nat. Commun., 2015, 6, 1–8.

[21]Q. Akkerman, S. Park, E. Radicchi, F. Nunzi, E. Mosconi, F. Angelis, R. Brescia, P. Rastogi, M. Prato, and L. Manna, Nano Lett., 2017, 17, 1924.

[22]L. Wu, H. Hu, Y. Xu, S. Jiang, M. Chen, Q. Zhong, D. Yang, Q. Liu, Y. Zhao, B. Sun, Q. Zhang and Y. Yin, Nano Lett., 2017, 17, 9, 5799–5804.

[23]M. Saidaminov, J. Almutlaq, S. Sarmah, I. Dursun, A. Zhumekenov, R. Begum, J. Pan, N. Cho, O. Mohammed and O. Bakr, ACS Energy Lett., 2016, 1, 4, 840–845.

[24]S. Seth and A. Samanta, J. Phys. Chem. Lett., 2018, 9, 1, 176–183.

[25]Y.-K. Jung, J. Calbo, J.-S. Park, L. Whalley, S. Kim and A. Walsh, J. Mater. Chem. A, 2019, 7, 20254-20261.

[26]Y. Wang and H. Sun, Progress in Quantum Electronics, 2018, 60, 1–29.

[27]A. Elsaesser and C. V. Howard, Advance 2d Drug Delivery Reviews, 2012, 64, 129–137.

[28]M. Bruchez, JR., M. Moronne, P. Gin, S. Weiss and A. P. Alivisatos, Science, 1998, 281, 2013-2016.

[29]J. Kamal, R. Gomes, Z. Hens, M. Karvar, K. Neyts, S. Compernolle and F. Vanhaecke, Phys. Rev. B, 2012, 85 (3), 035126.

[30]J. Shang and X. Gao, Chem. Soc. Rev., 2014, 43, 7267-7278.

[31]J. De Roo, M. Ibáñez, P. Geiregat, G. Nedelcu, W. Walravens, J. Maes, J. C. Martins, I. Van Driessche, M. V. Kovalenko and Z. Hens, ACS Nano, 2016, 10 (2), No. 2, 2071-2081.

[32]J. Maes, L. Balcaen, E. Drijvers, Q. Zhao, J. De Roo, A. Vantomme, F. Vanhaecke, P. Geiregat and Z. Hens, J. Phys. Chem. Lett., 2018, 9 (11), 3093–3097.

[33]Y. Tong, E. Bladt, M. F. Aygüler, A. Manzi, K. Z. Milowska, V. A. Hintermayr, P. Docampo, S. Bals, A. S. Urban, L. Polavarapu and J. Feldmann, Angew. Chem. Int. Ed., 2016, 55, 13887.

[34]Y. Bekenstein, B. A. Koscher, S. W. Eaton, P. Yang, and A. P. Alivisatos, J. Am. Chem. Soc., 2015, 137 (51), 16008–16011.

[35]A. Pan, B. He, X. Fan, Z. Liu, J. J. Urban, A. P. Alivisatos, L. He, and Y. Liu, ASC Nano, 2016, 10 (8), 7943–7954.

[36]A. G. Son, E.V. Krivogina, N. V. Romanov, M. Y. Presnyakov, S. S. Shapovalov and S. A. Kozyukhin, Russ. J. Inorg. Chem., 2019, 64, 1587–1591.

[37]S. Kondo, K. Amaya, S. Higuchi, T. Saito, H. Asada and M. Ishikane, Solid State Communications, 2001, 120 (4), 141-144.

[38]M. Nikl, E. Mihokova, K. Nitsch, F. Somma, C. Giampaolo, G. P. Pazzi, P. Fabeni and S. Zazubovich, Chemical Physics Letters, 1999, 306 (5-6), 280-284.

[39]M. N. Gulakov, N. Kh. Petrov, M. V. Alfimov and S. Techert, High Energy Chemistry, 2004, 38 (6), 381–386.

[40]IUPAC, Green Book, 2nd ed.: IUPAC Quantities, Units and Symbols in Physical Chemistry, Blackwell Scientific Publications, Oxford, 1993.

[41]Z. Hens and I. Moreels, J. Mater. Chem.,2012, 22 (21), 10406–10415.

[42]Y. Justo, P. Geiregat, K. Van Hoecke, F. Vanhaecke, C. De Mello Donega and Z. Hens, J. Phys. Chem. C, 2013, 117 (39), 20171–20177.

[43]A. W. Achtstein, A. Antanovich, A. Prudnikau, R. Scott, U. Woggon and M. Artemyev, J. Phys. Chem. C, 2015, 119 (34), 20156–20161.

[44]H. Htoon, J. A. Hollingworth, A. V. Malko, R. Dickerson and V. I. Klimov, Appl. Phys. Lett., 2003, 82 (26), 4776–4778.

[45]J. S. Owen, E. M. Chan, H. Liu and A. P. Alivisatos, J. Am. Chem. Soc., 2010, 132 (51), 18206–18213.

[46]S. Abe, R. K. Čapek, B. De Geyter and Z. Hens, ACS Nano, 2012, 6 (1), 42–53.

[47]J. Tauc, Ed. Abeles F. Amsterdam: North Holland, 1970.

[48]Q. A. Akkerman, S. Park, E. Radicchi, F. Nunzi, E. Mosconi, F. De Angelis, R. Brescia, P. Rastogi, M. Prato and Liberato Manna, Nano Lett., 2017, 17 (3), 1924–1930.

[49]M. Liu, J. Zhao, Z. Luo, Z. Sun, N. Pan, H. Ding and X. Wang, Chem. Mater., 2018, 30 (17), 5846–5852.

[50] S. Zou, C. Liu, R. Li, F. Jiang, X. Chen, Y. Liu and M. Hong, Adv. Mater., 2019, 31, 1900606.

[51]A.S. Hassanien and A.A. Akl, Superlattices and Microstructures, 2016, 89, 153-169.

[52]F. Urbach, Phys. Rev., 1953, 92 (5), 1324.

[53]D. Gau, I. Galain, I. Aguiar and R. Marotti, ChemRxiv. Cambridge: Cambridge Open Engage, 2022.

[54]S. Zeiske, O. J. Sandberg, N. Zarrabi, C. M. Wolff, M. Raoufi, F. Peña-Camargo, E. Gutierrez-Partida, P. Meredith, M. Stolterfoht and A. Armin, J. Phys. Chem. Lett., 2022, 13 (31), 7280–7285.

[55]S. Singh, C. Li, F. Panzer, K. L. Narasimhan, A. Graeser, T. P. Gujar, A. Köhler, M. Thelakkat, S. Huettner and D. Kabra, J. Phys. Chem. Lett., 2016, 7 (15), 3014–3021.

[56]S.D. Stranks, V.M. Burlakov, T. Leijtens, J.M. Ball, A. Goriely and H.J. Snaith, Physical Review Applied, 2014, 2, 034007.

[57]Y. Yamada, T. Nakamura, M. Endo, A. Wakamiya and Y. Kanemitsu, J. Am. Chem. Soc., 2014, 136 (33), 11610–11613.